High Temperature Transport Properties of Tetrahedrite Cu12–xMxSb4–yTeyS13 (M = Zn, Ni) Compounds

Yohan Bouyrie, Christophe Candolfi, Jean-Baptiste Vaney, Anne Dauscher, Bertrand Lenoir

High Temperature Transport Properties of Tetrahedrite $Cu_{12-x}M_xSb_{4-y}Te_yS_{13}$ (M = Zn, Ni) Compounds

Y. BOUYRIE, C. CANDOLFI, J.B. VANEY, A. DAUSCHER and B. LENOIR

Institut Jean Lamour, UMR 7198 CNRS – Université de Lorraine, Parc de Saurupt, CS 50840, 54011 Nancy, France.

ABSTRACT

Natural and synthetic tetrahedrites are currently focusing attention in thermoelectricity due to their earth's abundance, numerous possibilities of substitution and their complex crystal structure ($I\bar{4}3m$) resulting in extremely low lattice thermal conductivity (below 1 $W.m^{-1}.K^{-1}$ above 300 K). Here, we report on the synthesis, structural and chemical characterizations and high-temperature thermoelectric properties of polycrystalline $Cu_{12-x}M_xSb_{4-y}Te_yS_{13}$ (M = Zn, Ni) tetrahedrites. Upon substituting on both the Cu and Sb sites, we successfully improved the thermoelectric properties with respect to the ternary compound $Cu_{12}Sb_4S_{13}$ with peak ZT values of 0.7 at 700 K.

INTRODUCTION

For long, fossil energies have been put forward because of their high-energy conversion efficiency, but global environmental and energy issues have called for new environmentally friendly alternative energies. Among them, thermoelectricity is receiving attention because of its ability to harvest waste heat and convert it into electricity, without any pollution for the environment. The performance of a material to convert heat into electricity or vice-versa is related to its dimensionless thermoelectric figure of merit $ZT = \alpha^2 T / \rho\kappa$ [1, 2], which depends at the absolute temperature T on the thermopower (or Seebeck coefficient) S, the electrical resistivity ρ, and the total thermal conductivity κ ($\kappa = \kappa_E + \kappa_L$, where κ_E is the electronic thermal conductivity and κ_L the lattice thermal conductivity). In order to maximize the thermoelectric performances of a given material, high ZT values must be obtained by adjusting the three transport properties: high Seebeck coefficient, low electrical resistivity, and low thermal conductivity. Reducing the lattice thermal conductivity κ_L is one of the several strategies currently used to reach this goal.

Very recently, tetrahedrite compounds have been considered as possible candidates because of their naturally low lattice thermal conductivity and the possibility of adjusting their electrical properties by doping [3]. Natural tetrahedrite minerals possess a general chemical formula that may be written within a pure ionic picture as $A_{10}^{+}B_2^{2+}X_4^{3+}Y_{13}^{2-}$ where A is Cu or Ag, B is a metal such as Fe, Zn, Ni, Co, or Mn, X stands for Sb, As or Te and Y for S or Se. This family of compounds crystallizes into a body-centred cubic structure (space group $I\bar{4}3m$) that contains 58 atoms. The tetrahedrite structure was described by Wuench et al. [4] in 1964 (Fig. 1).

High-temperature thermoelectric properties (300 – 700K) of the ternary compound and its deratives have been reported [3, 5]. Compositions such as $Cu_{12-x}M_xSb_4S_{13}$ (with M = Fe,

Zn, Ni, Co, Mn) or $Cu_{12}Sb_{4-x}Te_xS_{13}$ have been studied. These studies revealed that these compounds behave as as *p*-type semiconductors [5, 6] and show very low thermal conductivity values of the order of 0.5 $W.m^{-1}.K^{-1}$ from 300 to 700 K. The favorable combination of these properties led to a maximum *ZT* of 0.85 at 700 K for the composition $Cu_{12}Sb_3Te_1S_{13}$.

However, even though double substitutions on the Cu site have been recently considered [7], substitutions on both the Cu and Sb sites remain so far unexplored. Herein, we report on the high-temperature thermoelectric properties of the series $Cu_{12-x}Zn_xSb_{4-y}Te_yS_{13}$ and $Cu_{12-x}Ni_xSb_{4-y}Te_yS_{13}$.

EXPERIMENTAL DETAILS

Stoichiometric amounts of elemental powders of high purities (Cu 99.99 %, Sb 99.999 %, S 99.999 %, Te 99.999 %, Zn 99.9999 % and Ni 99.995 %) were weighted and mixed for the desired compositions $Cu_{12-x}Zn_xSb_{4-y}Te_yS_{13}$ with (x,y) = (0.5, 1.0) ; (0.50, 1.25) and (1.0, 0.5) and $Cu_{12-x}Ni_xSb_{4-y}Te_yS_{13}$ with (x,y) = (0.5, 0.5) ; (0.50, 0.75) and (0.5, 1.0). For each composition, the mixed powders were loaded into an evacuated quartz tube and sealed under secondary vacuum (10^{-4} Pa). The tube was then placed into a vertical furnace, heated to 923 K, kept at this temperature for 12h and finally cooled down to room temperature. The resulting ingots were crushed into fine powders, cold-pressed into pellets and further annealed at 673 K for at least 14 days in sealed quartz tubes. The pellets were grounded into fine powders and densified in graphite dies by spark plasma sintering (SPS) at 723 K under 80 MPa for 12 min. The relative density of all samples was above 92% of the theoretical density.

Powder X-ray diffraction (PXRD) patterns were recorded to assess phase purity with a Bruker D8 Advance diffractometer equipped with a Ge (111) monochromator and using

$CuK\alpha_1$ radiation (λ = 1.54056 Å). The PXRD data were refined by the Rietveld method using the Fullprof software to determine the lattice parameter. The chemical homogeneity of the samples was verified by scanning electron microscopy (SEM) using a Quanta FEG (FEI). Images of the surface of the samples were collected in the backscattering electron mode (BSE) to contrast the tetrahedrite phase from impurity phases. X-ray elemental mapping was performed to assess the spatial distribution of the elements in the samples. The actual chemical compositions of the consolidated pellets were probed on polished surfaces by energy and wavelength dispersive spectroscopy (EDXS/WDXS) using a JEOL J7600F instrument. We used the chalcopyrite compound $CuFeS_2$ together with ZnS, Sb and Te as standards to determine the Cu, S, Sb and Te concentrations. In order to minimize matrix effects, both $CuFeS_2$ and ZnS were chosen due to the similar atomic environments of Cu and S in these structures with respect to those in tetrahedrites. The actual compositions were obtained from an average of 15 spots measured on the surface of each samples. The chemical formulae were normalized to 13 sulphur atoms (Table 1) since no deviations on this site have been reported so far.

Electrical resistivity and thermopower were measured simultaneously between 300 and 700 K with a ZEM-3 system (Ulvac-Riko). A careful determination of the thermal conductivity at high temperatures (300 – 700 K) was obtained by measuring the thermal diffusivity d by a laser flash technique (LFA 427, Netzsch) and the specific heat C_p with a differential scanning calorimeter (Pegasus 403 F3, Netzsch). The thermal conductivity was then calculated from $\kappa = dC_p\alpha_V$ where α_V is the experimental density of the sample whose temperature variation has been neglected in the present case.

RESULTS AND DISCUSSION

Structural and chemical characterizations

All the densified samples show a single tetrahedrite phase as revealed by the XRD patterns displayed in Fig. 2 for the illustrative $Cu_{11.5}Zn_{0.5}Sb_{3.5}Te_{1.0}S_{13}$ and $Cu_{11.5}Ni_{0.5}Sb_{3.5}Te_{0.5}S_{13}$ samples. The data were successfully refined within the $I\bar{4}3m$ space group of tetrahedrite for all compositions. For the Ni series, the lattice parameter quasi-linearly increases when the Te content increases, from 10.3314 Å for y = 0.5 to 10.3466 Å for y = 1.0. The same behavior is observed in the Zn series for which the lattice parameter increases from 10.3378 Å for (x,y) = (0.5, 1.0) to 10.3497 Å for (x,y) = (0.5, 1.25). These values are larger than that of the ternary compound $Cu_{12}Sb_4S_{13}$ (10.3293 Å, [8]). Consequently, the double substitution, Zn or Ni for Cu and Te for Sb, leads to an increase in the lattice parameter, in contrast with prior investigations on the $Cu_{12-x}Ni_xSb_4S_{13}$ [9] where the lattice parameter remains practically constant with x.

Figure 3 shows the SEM images of the $Cu_{11.5}Zn_{0.5}Sb_{2.75}Te_{1.25}S_{13}$ and $Cu_{11.5}Ni_{0.5}Sb_{3.25}Te_{0.75}S_{13}$ samples. In both cases, the results indicate the presence of a homogeneous matrix with a small proportion of secondary phases undetectable by PXRD. In the Zn containing samples, ZnS and $CuSbS_2$ could be detected while in the Ni containing samples, NiS_2 and $CuSbS_2$ were found. The presence of these secondary phases suggests that the actual compositions may slightly differ from the nominal compositions. In addition, the SEM data reveals that the solubility of Te into the matrix is higher than that of the elements substituting for Cu atoms (Zn, Ni).

As previously suggested, the actual compositions for both series deviate from the exact stoichiometry (see table 1). This off-stoichiometry is even more pronounced for the Cu_{12-}

$_x$Zn$_x$Sb$_{4-y}$Te$_y$S$_{13}$ samples. The insertion of Zn seems to compete with the addition of Te in the tetrahedrite matrix resulting in drastically lowered Zn concentrations. For the Cu$_{12-x}$Ni$_x$Sb$_{4-y}$Te$_y$S$_{13}$ samples, the actual Ni concentration is a slightly lower than the nominal one, while the actual Te concentration is very close to the nominal one. This tends to indicate that Te element integrates better the tetrahedrite matrix than transition metals when both are present.

Transport Properties

The thermoelectric properties were measured for all compounds over the 300 - 700 K temperature range as illustrated in Figure 4. Except for Cu$_{11}$Zn$_1$Sb$_{3.5}$Te$_{0.5}$S$_{13}$, each sample shows the same electrical and thermal behaviour with increasing temperature.

The ρ values (Fig. 4a) tend to slightly increase with T, indicative of a metallic character. ρ ranges between 30 and 90 μΩ.m at 673 K depending on the Te content and the nature of the element substituting for Cu (Zn or Ni). When the Te concentration increases, so does the ρ values in agreement with Morelli et al. [6]. Figure 4b shows that all samples exhibit positive thermopower values, indicating that holes are the majority charge carriers. *S* monotonically increases with temperature and reaches values that range between 150 and 210 μV.K^{-1} at 673 K. We note that the temperature dependence of the Seebeck coefficient of the (x, y) = (1.0;0.5) sample reveals a hump around 500 K whose origin remains so far unknown. This anomaly is not observed on Fig. 4a because of the logarithmic scale. The origin could be electronic or structural as demonstrated by Makovicky and Skinner [10] on the ternary composition Cu$_{12}$Sb$_4$S$_{13}$, or even due to decomposition of a secondary phase as highlighted on Fig. 3. Further PXRD measurements at high temperature may help solve this issue. Based on previous studies [5, 11], pure Cu$_{12}$Sb$_4$S$_{13}$ is a *p*-type metal. Adding elements such as Te, Zn, Ni, Co and Mn provides additional electrons to the tetrahedrite structure, thereby

progressively filling the valence bands and driving the compound to a semiconducting state. This scenario is consistent with our experimental results.

To verify that the nature of the element (Zn or Ni) substituting for Cu does not affect the electrical response of tetrahedrites, the electrical properties should be compared in samples with similar chemical compositions. However, in the present case, the compositions (*x,y*) : (0.5,0.5) and (*x,y*) : (0.50,0.75) could not be prepared for $Cu_{12-x}Zn_xSb_{4-y}Te_yS_{13}$ by our synthetic method. Both samples remained quite inhomogeneous, even after long-time annealing. Because of the significant fraction of impurity phases, these two samples were not further investigated.

The temperature dependence of the thermal conductivity, shown in Fig. 4c, reveals extremely low values, ranging between 0.6 and 0.8 $W.m^{-1}.K^{-1}$ in the temperature range investigated. The decrease in the thermal conductivity trends with the ($x + y$) content. An increase in ($x + y$) leads to an increase in the electrical resistivity and thus, to a decrease in the electronic contribution to the thermal conductivity.

As shown in Fig. 5, the Ni series present higher thermoelectric performance with respect to the Zn series. A maximum *ZT* value of 0.7 at 673 K was obtained for $Cu_{11.5}Ni_{0.5}Sb_{3.25}Te_{0.75}S_{13}$. This result indicates that double substitution in the tetrahedrite structure is a fruitful way of research to improve the thermoelectric properties of tetrahedrites [5, 9, 12]. However, there still exist other combinations of substitutions to test, in order to check whether the thermoelectric properties of tetrahedrites can be further enhanced.

CONCLUSION

In this work, we prepared two series of $Cu_{12-x}M_xSb_{4-y}Te_yS_{13}$ (M = Zn, Ni) compounds by direct melting of pure elements at high temperature followed by SPS sintering. PXRD showed no trace of contamination of the samples by any secondary phase, while SEM analyses revealed the presence of ZnS, NiS_2 and $CuSbS_2$. For all the studied compositions, both the thermopower and the electrical resistivity increase with temperature, whereas the thermal conductivity decreases. A maximum ZT value of 0.7 at 673 K was obtained for $Cu_{11.5}Ni_{0.5}Sb_{3.25}Te_{0.75}S_{13}$, higher than that of the ternary compound $Cu_{12}Sb_4S_{13}$ (0.6 at 700 K) but lower than those achieved in some quaternary tetrahedrites [5, 9, 12], which approach 1.0 at 700 K.

REFERENCE

1. Mahan, G.D., *Good Thermoelectrics.* 1997. **51**: p. 81-157.
2. Tritt, T.M., *Recent Trends in Thermoelectric Materials Research III*. 2001: Academic Press.
3. Suekuni, K., et al., *Thermoelectric Properties of Mineral Tetrahedrites Cu$_{10}$Tr$_{2}$Sb$_{4}$S$_{13}$ with Low Thermal Conductivity.* Applied Physics Express, 2012. **5**(5): p. 051201.
4. Wuensch, B.J., *The crystal structure of tetrahedrite, Cu12Sb4S18.* Zeitschrift für Kristallographie-Crystalline Materials, 1964. **119**(1-6): p. 437-453.
5. Lu, X., et al., *High Performance Thermoelectricity in Earth-Abundant Compounds Based on Natural Mineral Tetrahedrites.* Advanced Energy Materials, 2013. **3**(3): p. 342-348.
6. Lu, X. and D. Morelli, *The Effect of Te Substitution for Sb on Thermoelectric Properties of Tetrahedrite.* Journal of Electronic Materials, 2013. **43**(6): p. 1983-1987.
7. Lu, X., et al., *Increasing the thermoelectric figure of merit of tetrahedrites by Co-doping with nickel and zinc.* Chemistry of Materials, 2015. **27**(2): p. 408-413.
8. Pfitzner, A., M. Evain, and V. Petricek, *Cu12Sb4S13: A temperature-dependent structure investigation.* Acta Crystallographica Section B: Structural Science, 1997. **53**(3): p. 337-345.
9. Suekuni, K., et al., *High-performance thermoelectric mineral Cu12−xNixSb4S13 tetrahedrite.* Journal of Applied Physics, 2013. **113**(4): p. 043712.
10. Makovicky, E. and B.J. Skinner, *Studies of the sulfosalts of copper; VI, Low-temperature exsolution in synthetic tetrahedrite solid solution, Cu (sub 12+ x) Sb (sub 4+ y) S 13.* The Canadian Mineralogist, 1978. **16**(4): p. 611-623.
11. Suekuni, K., et al., *Systematic study of electronic and magnetic properties for Cu12–xTMxSb4S13 (TM = Mn, Fe, Co, Ni, and Zn) tetrahedrite.* Journal of Applied Physics, 2014. **115**(14): p. 143702.
12. Heo, J., et al., *Enhanced Thermoelectric Performance of Synthetic Tetrahedrites.* Chemistry of Materials, 2014. **26**(6): p. 2047-2051.

Table Captions

Table 1: Nominal and actual compositions of the $Cu_{12-x}Zn_xSb_{4-y}Te_yS_{13}$ and $Cu_{12-x}Ni_xSb_{4-y}Te_yS_{13}$ samples.

Figure Captions

Figure 1: Perspective view of the crystal structure of $Cu_{12}Sb_4S_{13}$.

Figure 2: Room-temperature Rietveld refinements of the X-ray diffraction patterns of the (a) $Cu_{11.5}Zn_{0.5}Sb_{3.5}Te_{1.0}S_{13}$ and (b) $Cu_{11.5}Ni_{0.5}Sb_{3.5}Te_{0.5}S_{13}$ compounds after densification by SPS. The experimental data are marked as red dots, the calculated pattern is in black and the difference between experimental and calculated patterns is shown in blue. The vertical green bars stand for the expected Bragg positions of the cubic crystal lattice of tetrahedrites.

Figure 3: SEM backscattered electron images collected on the $Cu_{11.5}Zn_{0.5}Sb_{2.75}Te_{1.25}S_{13}$ and $Cu_{11.5}Ni_{0.5}Sb_{3.25}Te_{0.75}S_{13}$ samples. The matrix is contaminated by secondary phases highlighted by a blue-triangle, a red-circle and a green-square for the $CuSbS_2$, ZnS and NiS_2 phases, respectively.

Figure 4: Temperature dependence of (a) electrical resistivity, (b) Seebeck coefficient and (c) thermal conductivity of the $Cu_{12-x}Zn_xSb_{4-y}Te_yS_{13}$ (red filled symbols) and $Cu_{12-x}Ni_xSb_{4-y}Te_yS_{13}$ (blue open symbols) compounds.

Figure 5: Temperature dependence of the dimensionless figure of merit *ZT* of the $Cu_{12-x}Zn_xSb_{4-y}Te_yS_{13}$ (red filled symbols) and $Cu_{12-x}Ni_xSb_{4-y}Te_yS_{13}$ (blue open symbols) compounds.

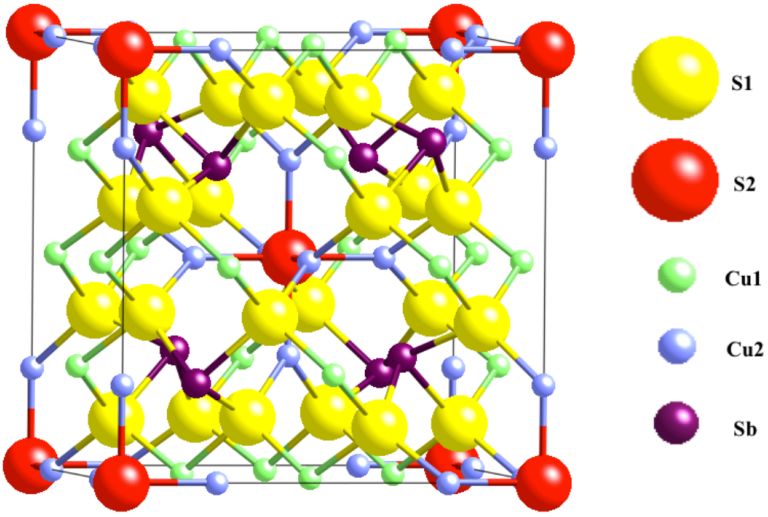

Figure 1

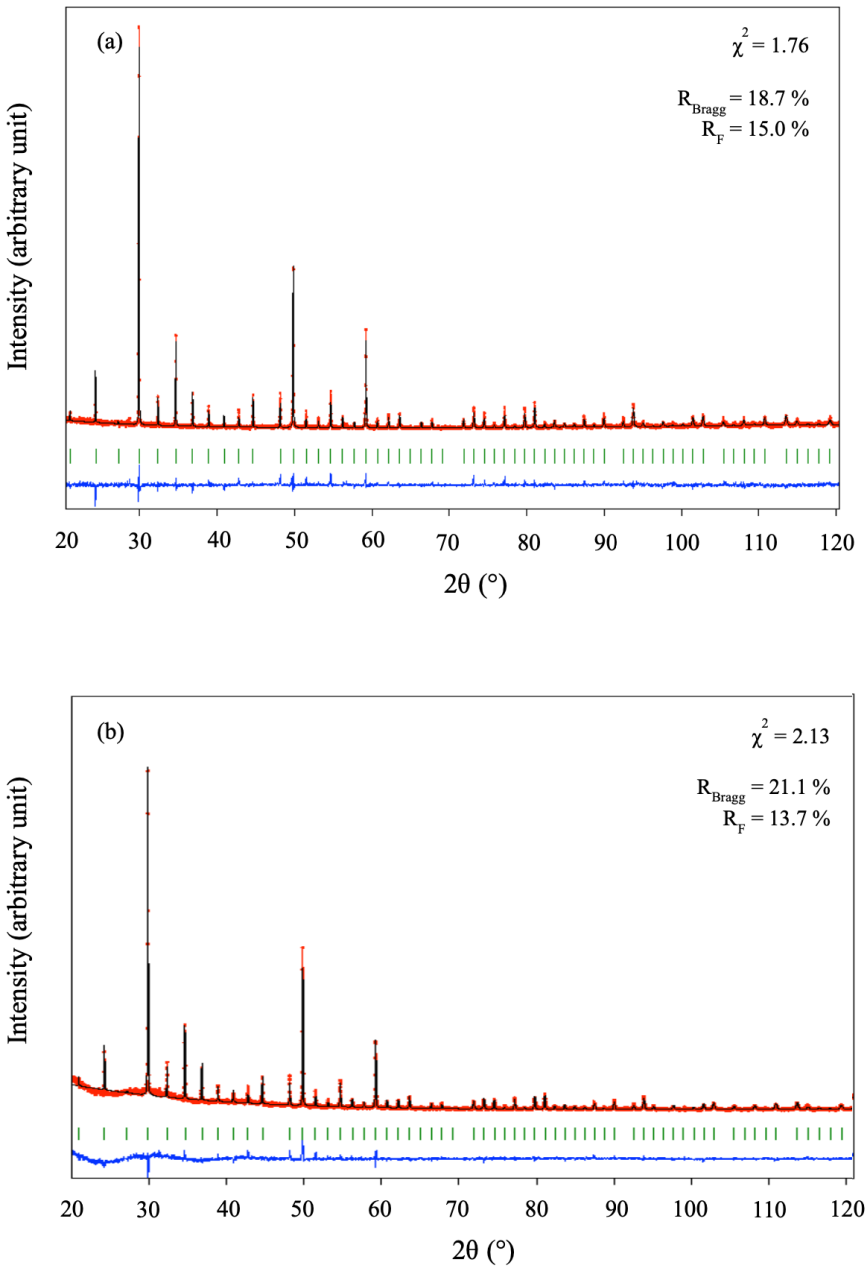
(a)
χ^2 = 1.76
R_{Bragg} = 18.7 %
R_F = 15.0 %
Intensity (arbitrary unit)
20 30 40 50 60 70 80 90 100 110 120
2θ (°)
(b)
χ^2 = 2.13
R_{Bragg} = 21.1 %
R_F = 13.7 %
Intensity (arbitrary unit)
20 30 40 50 60 70 80 90 100 110 120
2θ (°)

Figure 2

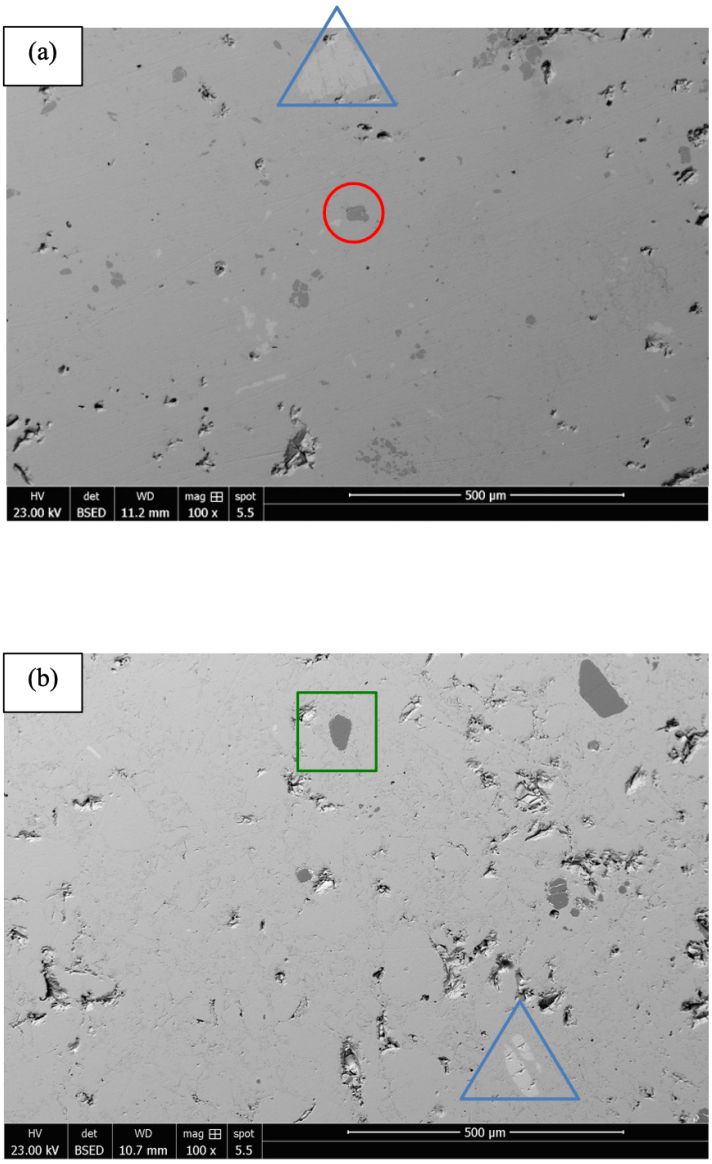
(a)
HV
23.00 kV
det
BSED
WD
11.2 mm
mag
100 x
spot
5.5
500 µm
(b)
HV
23.00 kV
det
BSED
WD
10.7 mm
mag
100 x
spot
5.5
500 µm

Figure 3

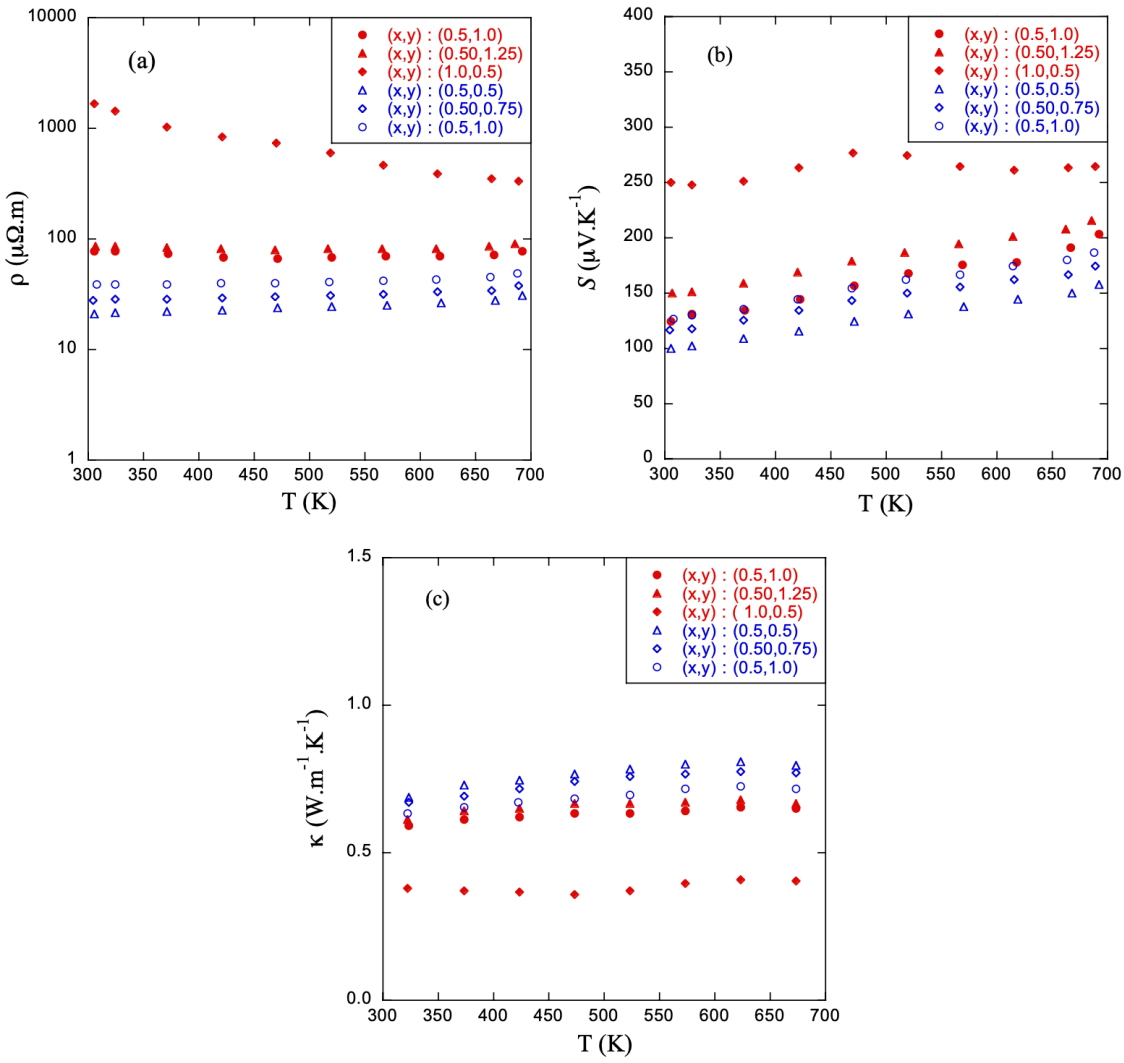
(a)
ρ (μΩ.m)
T (K)
(x,y) : (0.5,1.0)
(x,y) : (0.50,1.25)
(x,y) : (1.0,0.5)
(x,y) : (0.5,0.5)
(x,y) : (0.50,0.75)
(x,y) : (0.5,1.0)
(b)
S (μV.K-1)
T (K)
(c)
κ (W.m-1.K-1)
T (K)

Figure 4

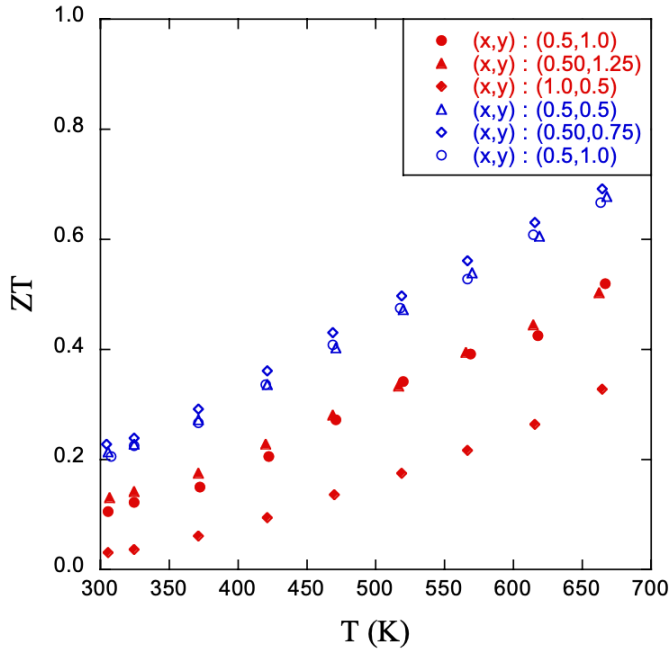
(x,y) : (0.5,1.0)
(x,y) : (0.50,1.25)
(x,y) : (1.0,0.5)
(x,y) : (0.5,0.5)
(x,y) : (0.50,0.75)
(x,y) : (0.5,1.0)
ZT
T (K)
0.0
0.2
0.4
0.6
0.8
1.0
300
350
400
450
500
550
600
650
700

Figure 5